Geomorphology 108 (2009) 219–233

Contents lists available at ScienceDirect

Geomorphology

journal homepage: www.elsevier.com/locate/geomorph

Susceptibility assessment of shallow landslides on Oahu, Hawaii, under extreme-rainfall events

Sanjit K. Deb [a], Aly I. El-Kadi [a,b,*]

[a] Water Resources Research Center, University of Hawaii at Manoa, Holmes, Hall 283, 2540 Dole Street, Honolulu, Hawaii 96822, USA
[b] Department of Geology and Geophysics, 1680 East-West Road, University of Hawaii at Manoa, Honolulu, Hawaii 96822, USA

ARTICLE INFO

Article history:
Received 12 August 2008
Received in revised form 17 January 2009
Accepted 21 January 2009
Available online 30 January 2009

Keywords:
Shallow landslide
SINMAP model
Slope stability
Oahu (Hawaii)

ABSTRACT

The deterministic Stability INdex MAPping (SINMAP) model, which integrates a mechanistic infinite-slope stability model and a hydrological model, was applied to assess susceptibility of slopes in 32 shallow-landslide-prone watersheds of the eastern to southern areas of Oahu, Hawaii, USA. Input to the model includes a 10-m Digital Elevation Model (DEM), an inventory of storm-induced landslides that occurred from 1949 to 2006, and listings of soil-strength and hydrological parameters including transmissivity and steady-state recharge. The study area of ca. 384 km^2 was divided into four calibration regions with different geotechnical and hydrological characteristics. All parameter values were separately calibrated using observed landslides as references. The study used a quasi-dynamic scenario of soil wetness resulting from extreme daily rainfall events with a return period of 50 years. The return period was based on almost-90-year-long (1919–2007) daily rainfall records from 26 raingauge stations in the study area. Output of the SINMAP model includes slope-stability-index-distribution maps, slope-versus-specific-catchment-area charts, and statistical summaries for each region.

The SINMAP model assessed susceptibility at the locations of all 226 observed shallow landslides and classified these susceptible areas as unstable. About 55% of the study area was predicted as highly unstable, highlighting a critical island problem. The SINMAP predictions were compared to an existing debris-flow-hazard map. Areas classified as unstable in the current study were classified as low-to-moderate and moderate-to-high debris-flow hazard risks by the prior mapping. The slope-stability maps provided by this study will aid in explaining the causes of known landslides, making emergency decisions, and, ultimately mitigating future landslide risks. The maps may be further improved by incorporating heterogeneous and anisotropic soil properties and spatial and temporal variation of rainfalls as well as by improving the accuracy of the DEM and the locations of shallow landslide initiation.

1. Introduction

Oahu, the third largest of the eight major islands of Hawaii, combines several essential components for the development of debris flows and rapid shallow landslides: steep hillsides with colluvial or regolith cover, heavy rainfalls, and strong demand for residential development in upland areas. Steep hillslopes are the dominant geomorphic feature of Hawaiian landscapes as deeply dissected, mature volcanic landscape (Moore and Mark, 1992). Landslides are the most important denudation process affecting watersheds dominated by steep slopes (Wentworth, 1943; Scott and Street, 1976; Li, 1988; Hill et al., 1997). Most of debris flows on the island of Oahu—variously referred to as debris avalanches, lahars, or mudflows (Campbell, 1975; Varnes, 1978; Ellen and Wieczorek, 1988)—typically begin on steep hillslopes, especially those near the crest of the Koolau Range and along other steep ridgelines. Intense rainfall triggers shallow landslides that transform into debris flows including soil, vegetation, and loose weathered bedrock that flow rapidly down hillslopes or stream channels (Wentworth, 1943; Scott, 1969; Scott and Street, 1976; Torikai and Wilson, 1992; Wilson et al., 1992; Ellen et al., 1991, 1993; Peterson et al., 1993; Kwong et al., 1999).

More than 1779 landslide scars were identified by systematic stereoscopic examination of 19 sets of aerial photographs of the Honolulu District, southeastern Oahu, between 1940 and 1989 (Peterson et al., 1993). Their study area extends from Moanalua Valley to Makapuu Point on north- and northwest-facing leeward hillslopes of the Koolau Range. The great majority of these landslides involve thin (0.1 to 1.5 m) slabs of hillside that consist largely of colluvial soil cover and vegetation. However, less common debris flows are also initiated by larger and deeper landslides that mainly involve weathered bedrock called saprolite. Peterson et al. (1993) reported

* Corresponding author. Water Resources Research Center, University of Hawaii at Manoa, Holmes, Hall 283, 2540 Dole Street, Honolulu, Hawaii 96822, USA. Tel.: +1 808 956 6331; fax: +1 808 956 5512.
E-mail addresses: sanjit@hawaii.edu (S.K. Deb), elkadi@hawaii.edu (A.I. El-Kadi).

0169-555X/$ – see front matter © 2009 Elsevier B.V. All rights reserved.
doi:10.1016/j.geomorph.2009.01.009

that the surface area of the landslide scars in the study area ranged from <10 to 5860 m^2 with a mean of 291 m^2. The average depth of 33 shallow-landslide scars, measured normal to the hillslope, ranged from 0.3 to 1.5 m with a mean of 0.79 m.

The severity of the shallow-landslide hazard on Oahu was again forcefully brought to the public's attention during the New Year's Eve 1987–1988 storm events in which more than 400 debris flows, mostly derived from shallow translational landslides, were triggered in southeastern and southern Oahu from Aina Haina to Kalama Valley (Dracup et al., 1991; Ellen et al., 1991). Debris flows from these landslides caused no fatalities but they struck and damaged numerous homes, utilities, and other infrastructure elements in Kuliouou and Hahaione valleys. The flows accumulated debris that diverted flood-waters and damaged streets and homes in Hahaione and Niu valleys (State of Hawaii, 1988; Federal Emergency Management Agency, 1988; Dracup et al., 1991). Damage from the storm was of sufficient severity and magnitude to warrant a federal disaster declaration (Federal Emergency Management Agency, 1988). In addition to damages reported from rapid landslides, since the mid-1950s damages from over a dozen slow landslides have been reported for homes, streets, and utilities in several valleys especially Aina Haina, Kuliouou, Manoa, and Palolo in southeastern Oahu (Peck, 1959, 1967, 1968; Peck and Wilson, 1968; Baum et al., 1989, 1990, 1991; Baum and Reid, 1992; Ellen et al., 1995; Wan and Kwong, 2002). Slow landslides have distinct head scarps at their upslope ends and distinct toes at downslope ends. Sliding depth is typically in the range of 3–15 m, but movement can be at depths as shallow as 5 m (Aina Haina) and as deep as 22 m (Palolo) (Ellen et al., 1995; Kaya and Kwong, 2007). Long-term average movement rates after the initial triggering event is generally less than 6 mm day^{-1}, which falls within the slow landslide velocity scale provided by Cruden and Varnes (1996).

Attempts at stabilizing slow landslides in Aina Haina (Peck and Wilson, 1968; Wan and Kwong, 2002) and Palolo Valley (Peck, 1959, 1967, 1968) have been unsuccessful. Both landslides continue to exhibit signs of movement (Ellen et al., 1995; Kaya and Kwong, 2007). Hydrologic monitoring of rainfall and pore-water pressure at these sites suggests that the surface soils of the main bodies of the landslide remain nearly saturated throughout the year and buried vertisols in the subsurface provide slope-parallel horizons of weak, highly plastic, expansive clay in which low permeability creates a favorable surface for perching groundwater (Johnsson et al., 1993; Ellen et al., 1995). Subsurface water pressure, which is a critical contributing factor for the development of soil slips, is directly related to the amount of rainfall (Baum and Reid, 1992), rainfall intensity and duration (Torikai and Wilson, 1992; Wilson et al., 1992), and seasonal patterns of rainfalls (Ellen et al., 1995).

Information pertinent to Oahu landslides is still limited, despite the fact that landslides, especially rapid shallow landslides, pose severe threats to life, infrastructure, and property. Fear of possible future landslides has become a major constraint on further property development. Annual landslide inventories are rarely done and there is almost no information on susceptibility or terrain-stability assessment with respect to landslide occurrence. Greater efforts are needed to understand landslide and terrain-stability processes, to analyze threatening landslide hazards, and to predict future landslides as accurately as possible to minimize damages. Geotechnical studies to assess landslide-susceptible areas and to stabilize landslide-prone areas through engineering construction can be both time-consuming and very expensive. Simple-but-reliable mathematical prediction tools for landslide susceptibility assessment would provide a viable planning and/or development alternative.

Some studies (e.g., Wilson et al., 1992; Torikai and Wilson, 1992) have revealed that widespread landslide activity and associated debris flows on Oahu are triggered when heavy rainfall, infiltrating into the subsurface, becomes impounded or forms a perched water table. This creates elevated pore-water pressures that cause a reduction in the shear strength of the soils. The failure surface is generally the contact surface between the soils (colluvium or regolith) and the bedrock. There are two primary methods of mathematically simulating such rainfall-triggered landslides (Casadei et al., 2003; Lan et al., 2004): 1) establishing empirical relationships between rainfall parameters and landslides by statistical correlations and forecasting techniques, and 2) simulating groundwater recharge and pore-water pressure changes associated with rainfall events by applying a deterministic model that couples a mechanical slope-stability model with a hydrological model. The latter approach is widely used for the assessment of shallow landslide susceptibility (Grayson et al., 1992a,b; Dietrich et al., 1992, 1993, 1995, 2001; Montgomery and Dietrich, 1994; Wu and Sidle, 1995; Pack et al., 1998a; Montgomery et al., 2000). Available models include the shallow-landslide model SINMAP (for "Stability INdex MAPping"—Pack et al., 1998a,b, 2005). Applicability of the SINMAP model to predict the spatial distribution of rainfall-triggered shallow landslides has been tested in a variety of landslide-prone areas under different geological and climate conditions (Morrissey et al., 2001; Zaitchik and van Es, 2003; Zaitchik et al., 2003; Calcaterra et al., 2004; Lan et al., 2004; Meisina and Scarabelli, 2007). These studies demonstrate successful SINMAP calibration and show that the model can be considered a reliable tool for the production of landslide susceptibility maps under specified rainfall conditions. However, the SINMAP model has not previously been tested in landslide-prone watersheds of tropical volcanic island environments, such as Hawaii, where watersheds are characterized by abundant moisture supply, heavy annual rainfalls, and steep terrain.

The objective of this study is to assess the shallow landslide susceptibility of slopes in the watersheds of eastern to southern areas of Oahu under extreme-rainfall events using the SINMAP model. The model considers that the shallow translational landsliding phenomena are controlled by shallow groundwater flow convergence. Although shallow translational landslides were not the only type of slope failure identified in the study area, the infinite-slope stability model that SINMAP deems appropriate and tends to be conservative for deep-seated failure situations.

Available historical data were used to test the SINMAP model in Hawaii. After such validation, model-developed landslide susceptibility maps may be used to aid in explaining causes of known landslides, making emergency decisions, and, ultimately, significantly mitigating future landslide hazards.

2. The SINMAP model

Full details of the SINMAP model are available in Pack et al. (1998b, 2005). A summary of the SINMAP modeling approach is provided in the following sections.

2.1. The infinite-slope stability model

SINMAP methodology is based upon the infinite-slope stability model (Hammond et al., 1992; Montgomery and Dietrich, 1994) that balances (with edge effects neglected) destabilizing components of gravity against stabilizing components of friction and cohesion on a failure plane parallel to the ground surface. Based on the infinite-slope form of the Mohr–Coulomb failure law as expressed by the ratio of stabilizing forces (shear strength) to destabilizing forces (shear stress) on a failure plane parallel to the surface, the safety factor (SF) calculation in SINMAP is:

$$SF = \frac{C_r + C_s + \cos^2\theta[\rho_s g(D - D_w) + (\rho_s g - \rho_w g)D_w]\tan\phi}{D\rho_s g \sin\theta\cos\theta} \quad (1)$$

where C_r is root cohesion (N m^{-2}), C_s is soil cohesion (N m^{-2}), θ is slope angle (°), ρ_s is wet soil density (kg m^{-3}), ρ_w is the density of water (kg m^{-3}), g is gravitational acceleration (9.81 m s^{-2}), D is the

vertical soil depth (m), D_w is the vertical height of the water table within the soil layer (m), and ϕ is the internal friction angle of the soil (°). θ is the arc tangent of the slope S, expressed as a decimal drop per unit horizontal distance. Fig. 1a illustrates the geometry assumed in Eq. (1). Soil thickness, h (m), and depth D are related as $h = D\cos\theta$, which produces the dimensionless form of the infinite-slope stability model:

$$SF = \frac{C + \cos\theta(1 - wr)\tan\phi}{\sin\theta} \quad (2)$$

where $w = D_w/D = h_w/h$ is the relative wetness, $C = (C_r + C_s)/(hp_s g)$ is the combined cohesion (root and soil) made dimensionless relative to the perpendicular soil thickness, and $r = p_w/p_s$ is the water-to-soil density ratio.

2.2. Topographic wetness index

The areas in which the soil cover has higher water content (and degree of saturation) tend to occur in convergent hollow areas of the hillslopes, and landslides usually originate in such areas (Montgomery and Dietrich, 1994). The parameter a (specific catchment area), which is defined as the upslope contributing area of catchment per unit contour length ($m^2\ m^{-1}$) (Fig. 1b), has been incorporated into SINMAP. This parameter is closely tied to hydrologic models that represent runoff generation by saturation from below (Beven and Kirkby, 1979; O'Loughlin, 1986; Grayson et al., 1992a,b).

According to these topographically-based wetness index models, the following assumptions are adopted in SINMAP: 1) shallow-lateral-subsurface flow (throughflow) advances along topographic gradients, implying that the contributing area to flow at any point is given by the specific catchment area defined from the surface topography (Fig. 1b); 2) lateral discharge at each point is in equilibrium with a steady-state recharge R ($m\ day^{-1}$); and 3) the capacity for lateral flux at each point is $T\ sin\ \theta$, where T is the soil transmissivity (the vertical integral of the hydraulic conductivity of soil and is determined by $T = (K_s) \times h$ [$m^2\ day^{-1}$], where K_s is the uniform hydraulic conductivity [$m\ day^{-1}$] of a soil mantle overlying relatively impermeable bedrock, and h is the thickness of the soil [m] above the failure surface). Assumptions 1 and 2 together imply that lateral discharge q, depth integrated per unit contour length, is estimated by $q = R \times a$ ($m^2\ day^{-1}$). With assumption 3 the relative wetness is expressed as:

$$w = \min\left(\frac{Ra}{T\sin\theta}, 1\right) \quad (3)$$

The relative wetness has an upper boundary of 1 with any excess assumed to form overland flow. As illustrated in Fig. 1a, the relative wetness defines the depth of the perched water table within the soil layer. The ratio R/T in Eq. (3) quantifies the relative wetness in terms of assumed steady-state recharge proportional to the soil's capacity for lateral drainage of water.

2.3. Stability index

The first step of defining the stability index (SI) is to incorporate the wetness index from Eq. (3) into the dimensionless SF of Eq. (2):

$$SF = \frac{C + \cos\theta\left[1 - \min\left(\frac{R}{T}\frac{a}{\sin\theta}, 1\right)r\right]\tan\phi}{\sin\theta} \quad (4)$$

The topographic variables a and θ are derived from a Digital Elevation Model (DEM), whereas the values of C, $\tan\phi$, r, and R/T are user input. The parameter r is essentially treated as constant (with a value of 0.5) but the uncertainty in other three variables (C, $\tan\phi$, and R/T) is allowed through the specification of upper and lower boundaries. These boundaries define uniform probability distributions over which these parameters are assumed to vary at random. Denoting $R/T = x$, $\tan\phi = t$, and the uniform distributions with upper and lower boundaries as $C \sim U(C_1, C_2)$, $x \sim U(x_1, x_2)$, and $t \sim U(t_1, t_2)$, the probability is evaluated over the distributions of C, x, and t. SINMAP incorporates the probabilistic approach described by Hammond et al. (1992), while combining the infinite slope stability model with the steady state hydrology approach suggested by Montgomery and Dietrich (1994). The smallest C and t (i.e., C_1 and t_1) together with the largest x (i.e. x_2) defines the worst-case (most conservative) scenario under the assumed uncertainty (variability) in the parameters. Areas under this worst-case scenario where SF is greater than 1 are, according to this model, unconditionally stable. Where $SI = \text{Prob}(SF > 1)$, SI is defined as the minimum deterministic SF:

$$SI = SF_{\min} = \frac{C_1 + \cos\theta\left[1 - \min\left(x_2\frac{a}{\sin\theta}, 1\right)r\right]t_1}{\sin\theta} \quad (5)$$

For areas where the minimum SF is less than 1, there is a probability of failure. Such a probability is spatially variable due to the uncertainty in C, $\tan\phi$, and T. This probability also includes temporal variability in the parameter R, characterizing wetness that may vary with time. In these regions (with $SF_{\min} < 1$), $SI = \text{Prob}(SF > 1)$ over the distributions of C, x, and t. The best-case scenario is when $C = C_2$, $x = x_1$, and $t = t_2$, which leads to:

$$SI = SF_{\max} = \frac{C_2 + \cos\theta\left[1 - \min\left(x_1\frac{a}{\sin\theta}, 1\right)r\right]t_2}{\sin\theta} \quad (6)$$

In the case that $SF_{\max} < 1$, $SI = \text{Prob}(SF > 1) = 0$.

3. Application of the SINMAP model

3.1. Study area

The study area, covering ca. 384 km^2, includes 32 landslide-prone watersheds of the eastern to southern areas of Oahu. It extends from Moanalua Valley to the Koko Crater watershed on the leeward (southwest) side and from the Keaahala to Makapuu watersheds on

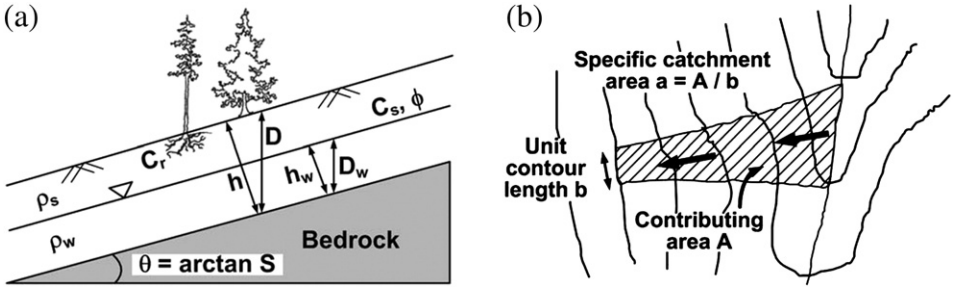

Fig. 1. Diagrams illustrating (a) the geometry of the assumed infinite-slope stability model and parameters involved in the safety factor in Eq. (1), and (b) the definition of specific catchment area.

the windward (northeast) side of the Koolau Mountain Range (Fig. 2). The geology of the study areas is the end result of shield-building volcanism, subsidence and slope failure, weathering, erosion, sedimentation, and rejuvenated volcanism. The Koolau Range, about 2.6 million year old mountain range (Carson and Clague, 1995), is the eroded remnants of the larger and younger of two major coalesced shield volcanoes that formed the Island of Oahu (Stearns and Vaksvik, 1935). The volcanic activity originating from fissures in a northwest-tending rift zone of the Koolau Shield Volcano built up the Koolau Range (Macdonald et al., 1983). Weathering and erosion have modified the original domed surfaces of the Koolau shield volcano, leaving a landscape of deep valleys and steep interfluvial ridges in the interior highlands that are mantled with colluvial deposits. Lithology of the study area consists mainly of basalt that was extruded in numerous gently dipping, thin (<3 m) flows of aa and pahoehoe lava (Visher and Mink, 1964). A major geomorphological evolution process in the study area is slope retreat from rainfall and stream formation (Scott and Street, 1976). The much steeper slopes on the windward side of the Koolau Range as compared to the leeward side are primarily the results of erosion of about 2 million years from orographic rainfall combined with stream cutting (Macdonald et al., 1983).

The study area consists of a series of steeply sloping valleys (with some slopes steeper than 80°) that extend from the Koolau Range crests, at a height of more than 950 m, down to the sea coast. Slopes consisting primarily of colluvium, and residual soils and completely weathered materials are susceptible to rainfall-induced failures (Kwong et al., 1999). Mean annual precipitation has a steep orographic gradient and varies widely in the study area. The windward slopes of the Koolau Range typically receive more rain than the leeward slopes as the moist air of the northeasterly trade wind loses its moisture through rainfall as it ascends the windward side of the mountain range. Based on records from a network of 13 raingauge stations (1916–1983), mean annual precipitation within the study area ranges from less than 650 mm in the southern and southwestern lowlands to more than 7000 mm over the highest part of the Koolau Range (Giambelluca et al., 1986). The winter months, October through April, generally receive more rainfall than the summer months. Streams in the study area are short and have steep gradients, and drain small catchments. These topographic characteristics favor the rapid concentration of runoff and the generation of flash floods.

Most valleys and some ridge crests below an altitude of ca. 305 m are urbanized. Residential development covers ca. 50% of the Honolulu District, which extends from Moanalua Valley to the Koko Crater watershed on the leeward side of the Koolau Range (Torikai and Wilson, 1992). The remainder of the district is undeveloped and is mostly designated as watershed or conservation land by the state. Honolulu is heavily urbanized and densely populated. Based on the National Oceanic and Atmospheric Administration (NOAA) Coastal Change Analysis Program (C-CAP) (NOAA, 2000), the eastern and southern areas of Oahu are also quite urbanized and characterized by resort developments.

Because of the wide variety of terrain types and rainfall distribution, the study area was divided into four calibration regions based on soil depth, soil texture, land cover (i.e., scrub/shrub, high- and low-density developed, evergreen forest and grassland), lithology, and whether or not a calibration region has inventoried historical shallow landslides (Fig. 2). Calibration regions are areas within which single lower and upper bound calibration parameter values can represent R/T, dimensionless cohesion, and friction-angle values required for the SINMAP application (Pack et al., 1998b, 2005). SINMAP uses a single soil density ratio parameter for each calibration region. Four calibration

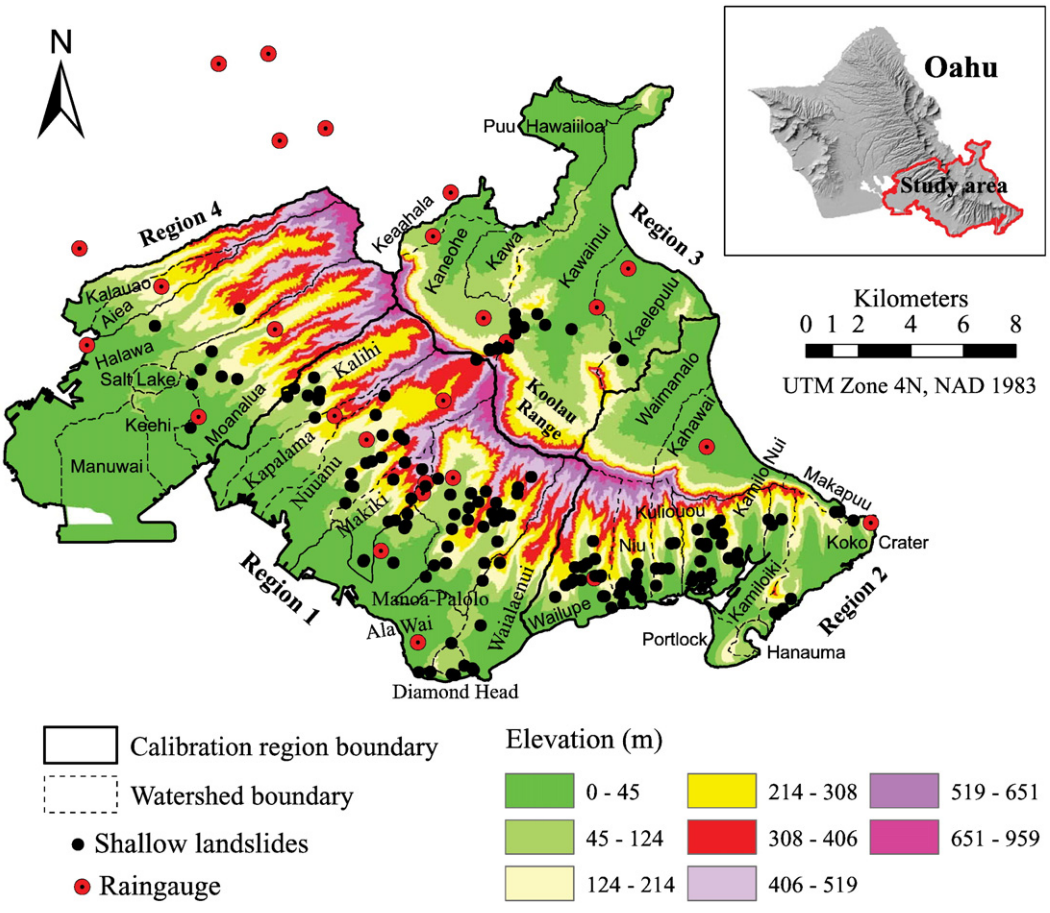

Fig. 2. Location of the study area and topographic map including the locations of 226 inventoried shallow landslides during the periods 1949–2006.

regions were defined using soils, lithologic-group distribution, and land use maps to identify areas having consistent calibration parameters. Calibration regions 1 to 4 have areas of ca. 114, 83, 85, and 103 km^2, and include 8, 11, 6, and 7 watersheds, respectively.

A description of major rock types and lithologic-group distributions, slope ranges, soil textural groups (United States Department of Agriculture [USDA], 1972), major land-cover types (C-CAP), and a debris-flow hazard rating (Ellen et al., 1993) for each of the four calibration regions is given in Table 1. The information in the table was derived from the USGS (United States Geological Survey) database of Oahu including geological maps, Soil Survey Geographic (SSURGO) maps, the USDA Natural Resources Conservation Service database of Oahu, the NOAA database of Oahu including the C-CAP maps and DEM, and the hazard-zonation maps for debris flows throughout most of the Honolulu District mapped by Ellen et al. (1993). These authors produced debris-flow hazard maps using digital simulations of debris flows within a 10-m DEM derived from USGS 1:24,000-scale topographic maps. Simulations, representing 10,000 years of debris-flow events, were based on the following.

- distribution and frequency of soil slips that generate debris flows, which were estimated from the rate of erosion of the 1.8-million-year-old Koolau volcanic dome combined with logistic regression of locations of mapped soil slips on hillslope steepness;

Table 1
Description of major lithologic-group distributions, slope ranges, soil textural groups (USDA, 1972), major land-cover types (C-CAP), and a debris-flow hazard rating for each of the four calibration regions in the landslide-prone study areas.

Region (area in km^2)	Watersheds (area in km^2)	Major lithologic groups distribution (% of the region area)	Slope range (% of the region area)	Major soil textural groups distribution (% of the region area)	Major land-cover types (% of the region area)[a]	Debris-flow hazard[b]
Region 1 (114.39)	Manoa-Palolo (25.28)	Lava flows, pahoehoe ropy lava, and aa clinkery lava (52.92)	0–6° (39.19)	Silty clay to silty clay loam (28.29)	Scrub/shrub (32.85)	Moderate to high[c]
	Nuuanu (24.47)	Alluvium and older alluvium sand and gravel (24.43)	6–15° (17.72)	Clay and clay loam to silty clay loam (24.44)	High-intensity developed (23.63)	
	Ala Wai (16.59)	Vent deposits (7.46)	15–25° (12.76)	Silty clay loam to very fine sandy loam (7.42)	Evergreen forest (18.61)	
	Kalihi (16.09)	Manmade fill (6.35)	25–35° (12.88)	Stratified gravelly sand to silty clay (7.42)	Low-intensity developed (18.39)	
	Waialaenui (15.48)		35–45° (12.01)	Stony clay (7.00)	Grassland (5.03)	
	Kapalama (8.66)		45–82° (5.43)			
	Makiki (6.83)					
	Diamond Head (1.00)					
Region 2 (82.61)	Waimanalo (15.33)	Lava flows, pahoehoe and aa (45.63)	0–7° (36.48)	Silty clay to silty clay loam (35.81)	Scrub/shrub (50.84)	Low to moderate[d]
	Wailupe (13.17)	Alluvium and older alluvium sand and gravel (28.52)	7–16° (17.38)	Clay and clay loam to silty clay loam (12.75)	Low-intensity developed (14.78)	
	Kahawai (11.96)	Vent deposits, coarse	16–26° (14.91)	Unweathered bedrock (10.00)	Evergreen forest (10.51)	
	Kamilo Nui (10.79)	Near-vent cinder and spatter (10.00)	26–36° (16.07)	Silt loam to silty clay loam (7.33)	Grassland (10.17)	
	Koko Crater (9.42)	Dike complex (4.45)	36–47° (11.09)	Stony clay (7.29)	High-intensity developed (9.00)	
	Niu (6.92)	Sand dunes, calcareous well-sorted sand (4.00)	47–76° (4.07)			
	Kamiloiki (6.13)					
	Kuliouou (4.68)					
	Portlock (1.88)					
	Makapuu (1.32)					
	Hanauma (1.01)					
Region 3 (84.63)	Kawainui (38.06)	Alluvium and older alluvium sand and gravel (35.78)	0–6° (46.13)	Silty clay to silty clay loam (38.70)	Scrub/shrub (29.48) Evergreen forest (22.05)	Not evaluated
	Kaneohe (14.73)	Lava flows, pahoehoe and aa (17.55)	6–14° (21.89)	Silty clay (12.38)	Low intensity developed (21.34)	
	Kaelepulu (14.03)	Dike complex (15.07)	14–24° (14.33)	Sand to coarse sand (8.00)	Grassland (10.44)	
	Puu Hawaiiloa (9.40)	Wall rock with more than 30% intrusions (6.39)	24–35° (9.67)	Clay and clay loam to silty clay loam (7.00)	High intensity developed (10.19)	
	Kawa (5.41)	Beach deposits, well-sorted sand and gravel (6.00)	35–50° (5.04)	Stratified gravelly sand to silty clay (6.00)		
	Keaahala (3.00)	Limestone and mudstone, reef deposits, and estuarine sediment (5.00)	50–79° (3.02)			
Region 4 (102.63)	Halawa (36.37)	Lava flows, pahoehoe and aa (49.07)	0–5° (42.16)	Clay and clay loam to silty clay loam (22.86)	Scrub/shrub (33.66)	Low to moderate[d]
	Moanalua (27.43)	Tuff (15.02)	5–13° (15.56)	Silty clay to silty clay loam (21.56)	High-intensity	
	Manuwai (17.04)	Manmade fill (13.16)	13–24° (10.63)	Stratified gravelly sand to silty clay (21.16)	Developed (20.88)	
	Kalauao (8.54)	alluvium and older alluvium sand and gravel (13.02)	24–34° (12.37)	Clay to weathered bedrock (9.28)	Low-intensity developed (18.20)	
	Keehi (6.39)	Limestone and mudstone, reef deposits, and estuarine sediment (7.23)	34–43° (12.68)		Evergreen forest (15.42)	
	Aiea (5.27)		43–72° (6.59)		Grassland (9.00)	
	Salt Lake (1.59)					

[a] High-intensity developed includes highly developed upland areas where people reside or work in high numbers, and impervious surfaces account for 80 to 100% of the total land cover. Low-intensity developed includes upland areas with a mixture of constructed materials and vegetations, and impervious surfaces account for 21 to 49% of the total land cover.

[b] High, moderate, and low hazard along the Koolau Range, designating as the relative degree of hazard from hillslope debris-flows of average size and travel-distance behavior that corresponds to return periods of 500 years or less, 501 to 2000 years, and 2001 to 10,000 years, respectively (Ellen et al., 1993).

[c] Moderate hazard is common on hillslopes and in places extends into suburban valley margins, particularly near mouths of steep sidehill drainages and where development has extended up valley walls; high hazard is common in steep drainages but is rare at roads or in suburban valley areas.

[d] Low hazard occurs more commonly in suburban valley margins of the study area.

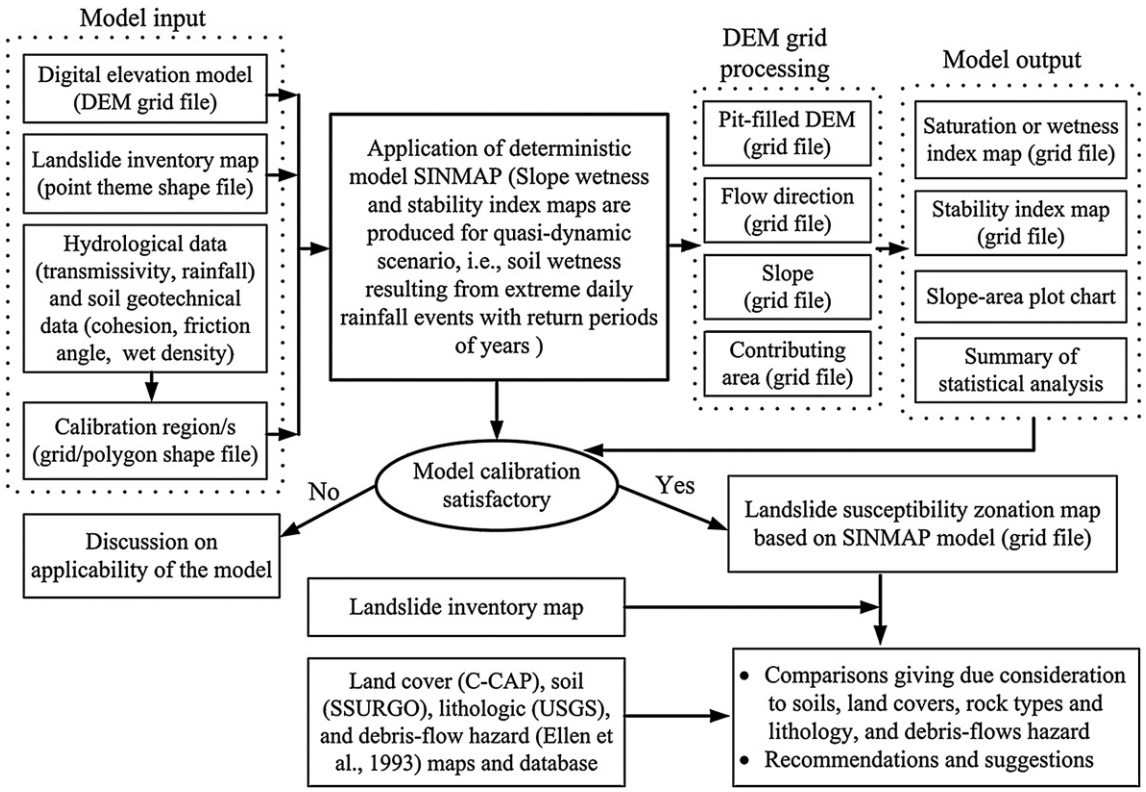

Fig. 3. Schematic diagram of the methodology used to apply SINMAP to the study under extreme-rainfall events.

- volume of soil slips, which was estimated from volumes of 201 soil-slip scars measured or estimated in the field and on aerial photographs; and
- travel-distance behavior of debris flows, which was estimated based on the change of the rate of debris-flow volume. The influence of topographic controls and vegetation on such a rate was quantified through a stepwise multiple regression approach using a sample of 26 debris flows on Oahu.

Mapped hazard areas included most of the previously mapped historical debris-flow paths, and the average frequency of debris flows was in general agreement with the historical record.

3.2. Model parameterization and calibration

SINMAP version 2.0 is an ArcGIS extension of the Environmental Systems Research Institute (ESRI) that implements the computation and mapping of a slope-stability index based on the mathematical scheme outlined above. The model uses the surface topography to route flow downslope, assuming that the subsurface hydrologic boundary (or bedrock-drift boundary) parallels the surface and the hydraulic conductivity of a soil mantle overlying impermeable bedrock is uniform. The flow model predicts relative levels of the perched water table across a watershed area characterizing subsurface flow through the colluvium or regolith. This prediction is then used to assess slope stability. Fig. 3 shows a schematic diagram of the methodology used for applying the SINMAP model. SINMAP calculations require a DEM, a map of observed landslides, and the values of calibration parameters.

Data needed for model development and calibration include the range of cohesion values, soil-density values, range of internal friction-angle values, and range of R/T ratios. By adopting suitable ranges for variables it is possible to calibrate and group the majority of observed landslides into the smallest *SI* classes (Table 2). The calculations are expressed by *SI* based on values of *SF* ranging from 0 to >1.5 (Pack et al., 1998b, 2005). During the calibration process all parameter values were adjusted separately for each calibration region. This procedure included an interactive calibration based on visual qualitative assessment, adjusting parameters using observed

Table 2
Classes of slope stability based on value of the Stability Index (*SI*), as set by the deterministic slope-instability model SINMAP.

Condition	Class	Predicted state	Parameter range	Possible influence of factors not modeled	Reclassified predicted state
$SI>1.5$	1	Stable slope zone	Range cannot model instability	Significant destabilizing factors are required for instability	Safe area
$1.5>SI>1.25$	2	Moderately stable slope zone	Range cannot model instability	Moderate destabilizing factors are required for instability	Low-to-medium susceptibility
$1.25>SI>1.0$	3	Quasi-stable slope zone	Range cannot model instability	Minor destabilizing factors are required for instability	
$1.0>SI>0.5$	4	Lower threshold slope zone	Pessimistic half of range required for instability	Destabilizing factors are not required for instability	High susceptibility
$0.5>SI>0.0$	5	Upper threshold slope zone	Optimistic half of range required for instability	Stabilizing factors may be responsible for stability	Very high susceptibility
$0.0>SI$	6	Defended slope zone	Range cannot model stability	Stabilizing factors are required for stability	

Table 3
Selected storm periods, 1949–2006, causing shallow landslides or debris slides in the study areas.

Year	Storm period	Geographic area	Total number of inventoried shallow landslides
1949	Jan 16–20	Nuuanu	1
1950	Dec 2–6	Aina Haina, Makapuu Point, St. Louis Heights, and Tantalus	7
1951	Mar 10–13	Diamond Head, Makiki, Maunalani Heights, Moiliili, Palolo, and Pauoa	8
1951	Mar 24–28	Makapuu Point and Nuuanu Pali	6
1958	Mar 5–6	Aina Haina, Diamond Head, Kalihi, Kuliouou, Manoa, Moanalua, Moiliili, Maunalani Heights, Niu, Nuuanu, Nuuanu Pali, Palolo, and St. Louis Heights	43
1963	May 14–15	Manoa, Moanalua, and Nuuanu	4
1965	Feb 3–4	Aina Haina, Koko Head, and Moanalua	4
1965	Nov 10–14	Aina Haina, Diamond Head, Halawa, Kalihi, Makiki, Manoa, Mapunapuna, Moanalua, Nuuanu, Nuuanu Pali, Palolo, and Tantalus	30
1967	Dec 17–18	Aina Haina, Makapuu Point, Manoa, Palolo, and Waialae	12
1969	Jan 31–Feb 2	Nuuanu Pali	2
1976	Feb 5–8	Kalihi and Pauoa	4
1977	May 11–14	Nuuanu Pali	3
1978	Oct 30–31	Diamond Head and Nuuanu Pali	2
1980	Jan 7–11	Diamond Head, Kailua, and Kaneohe	8
1981	May 6–7	Hahaione	6
1982	Jan 20–21	Diamond Head, Kailua, Kamilo Nui, Manoa, Maunawili, Nuuanu, and Nuuanu Pali	10
1985	Feb 12–14	Maunawili and Nuuanu Pali	3
1987-1988	Dec 30–Jan 1	Aina Haina, Hahaione, Hawaii Kai, Kaluanui, Kuliouou, Manoa, Maunawili, Moanalua, Niu, Nuuanu Pali, Palolo, and Pauoa	42
1989	Mar 31–Apr 2	Niu	2
1991	Mar 17–24	Aina Haina, Diamond Head, Kailua, Kamiloiki, Koko Crater, Kuliouou, Makapuu Point, Niu, Nuuanu, Nuuanu Pali, Paiko Peninsula, Tantalus, and Waialae	21
2003	May 20–23	Kailua and Nuuanu Pali	1
2003	Jun 2–3	Kailua and Nuuanu Pali	5
2006	Mar 25	Manoa	2

landslides as references. As suggested by Pack et al. (2005), the adjustment of parameters was performed such that the stability map captured a high proportion of observed landslides in regions with low stability index values, while minimizing the extent of low stability regions and subsequent alienation of terrain to regions where landslides have not been observed. Model outputs include stability probabilities expressed as stability indices, topographic wetness indices, graphs of landslide occurrences within slope-specific catchment area spaces, and summary tables of statistical analyses. The slope-specific catchment area graph provides the following information to aid in data interpretation and parameter calibration: (1) specific catchment area versus slope plotted for a sampling of grid cell points that does not have landslides; (2) landslides plotted based on values of the slope and specific catchment area of the cell in which each landslide point lies; (3) five stability index region lines (Table 2) providing boundaries for regions within slope-specific catchment area space that have similar potential for stability or instability; and (4) three saturation region lines (i.e., saturation, partially wet and low moisture, and threshold saturation lines) providing boundaries for regions within slope-specific catchment area space that have similar wetness potential.

3.2.1. Inventory of past landslides

Accurate positioning of the initiation locations of known shallow landslides is an essential element for a successful SINMAP calibration. We considered three sources of information for selected storm periods from 1949 to 2006 (Table 3) for the compilation of an inventory map of shallow landslides:

(1) A historical catalog of landslide events, compiled by searching available publication archives and a large number of newspaper issues;
(2) A geomorphological landslide inventory map, compiled from various studies that recognized shallow-landslide scars or debris slides. Data were compiled through stereoscopic interpretation of multi-temporal vertical aerial photographs. Analysis was aided by recognizing topographic features indicative of landslides on aerial photographs and topographic maps and by field verification of landslide data;
(3) Inventory maps of recent landslide events (e.g., 2003 and 2006), obtained by interpreting aerial photographs taken after a period of prolonged rainfall and by compiling information from newspaper articles and USGS reports.

The historical landslide catalogue was produced from information obtained from the Oahu Civil Defense Agency (OCDA), local government publications, USGS reports, and Honolulu's two daily newspapers (*The Honolulu Advertiser* and *Honolulu Star-Bulletin*). Reports of possible landslide scars and resulting debris flows were summarized by Torikai and Wilson (1992) for 23 selected Oahu storms over the period of 1935–1991. Torikai and Wilson (1992) compiled the OCDA debris-flow reports available for the time period 1959–1991 from communication logs written during civil defense emergencies such as heavy rainfall and flooding. Written logs recorded transcriptions of telephone calls to OCDA by residents and by civil defense officials at the emergency sites. The OCDA logs also included the dispatches by the Honolulu Police Department, Honolulu Fire Department, and National Weather Service (NWS). Other available studies and field observations presenting historical landslide inventories and aerial photographs include Wentworth (1943), Scott (1969), Scott and Street (1976), Ellen et al. (1991, 1993, 1995), Wilson et al. (1992), and Peterson et al. (1993).

Although great care was taken in compiling and analyzing available data, information used for preparing the landslide-inventory map is subject to a high degree of uncertainty because of a number of factors. The information was compiled from sources having few explanatory notes concerning the exact initiation location of the landslides. Although shallow landslides and the resulting debris flows occurred both on natural and manmade hillslopes, distinctions could not be made between the two hillslope types because of uncertainty regarding their exact locations (Torikai and Wilson, 1992). The data list may not be fully comprehensive or representative of actual landslides, considering that most of the identified landslides and resulting debris flows only addressed occurrences that encroached on residential developments or farm lots. The issue regarding accurate representation is certainly critical considering that the landslide inventory may have some bias towards developed areas in which the accounts are much more frequent.

The inventory map of a total of 226 shallow landslides, as shown in Fig. 2, was prepared as an ArcGIS point theme overlaid on USGS 7.5-minute 1:24,000-scale Digital Raster Graphic (DRG) topographic maps. All 226 inventoried landslides were classified as “debris slides”, meaning that they are shallow, translational, and composed of a mixture of coarse- and fine-grained soils. A total of 88, 85, 45, and 8 shallow landslides were inventoried for calibration regions 1, 2, 3, and 4, respectively.

3.2.2. Topographic data

A topographic map of the study area is shown in Fig. 2. Data used in the SINMAP were derived from a 10-m DEM of Oahu produced by the Center for Coastal Monitoring and Assessment Biogeography Branch, National Ocean Service, NOAA, Department of Commerce. The DEM for Oahu has a coordinate system of NAD (North American Datum) 83

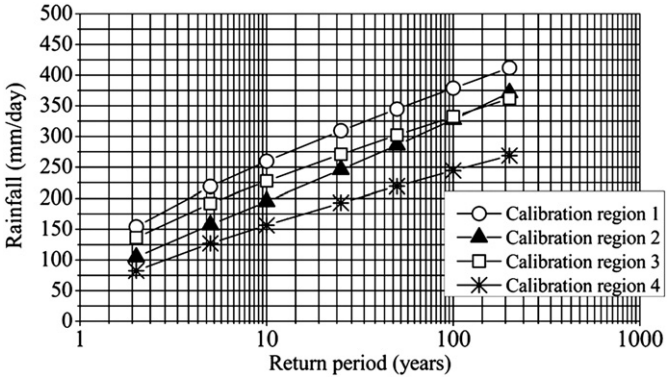

Fig. 4. Daily rainfall frequency analysis for different calibration regions (years 1919–2007) using a Log-Pearson Type III distribution to derive the maximum expected daily rainfall event for studying the quasi-dynamic scenario in SINMAP application, i.e., soil wetness resulting from extreme daily rainfall events with different return periods.

UTM (Universal Transverse Mercator) 4N. All raster data have a spatial resolution of 10 m and are in the ESRI grid format.

3.2.3. Hydrological data

Hydrological data needed for the model includes a wetness index defined as the ratio of transmissivity over steady-state recharge (T/R). Soil maps in the SSURGO database, the most detailed level of soil geographic data on the Island of Oahu, consist of georeferenced digital data and computerized attribute data in a 7.5-minute quadrangle format at a 1:24,000 scale. The SSURGO maps include a detailed, field-verified inventory of soils and non-soil areas that normally occur in a repeatable pattern on the landscape. Soil maps in the SSURGO database are made by field methods that require direct observations along traverses and field transects. Map unit composition and the positional accuracy of digital data are determined by these observations, using base maps that meet National Map Accuracy Standards. The SSURGO maps and database for Oahu list the upper and lower boundaries of permeability values of soils. These boundaries were used for calculating the transmissivity values.

The depth of a shallow landslide is generally not more than 1–2 m. Soil-thickness and moist-bulk-density values of soils were extracted from the SSURGO database for each watershed. The SSURGO maps and database also provided the basis for the study of soil properties. As also observed in several field studies (Baum et al., 1990, 1991; Baum and Reid, 1992; Ellen et al., 1995), the thickness of the soil above the failure surface varies within the study area. This variability was addressed by dividing the study area into different calibration regions with different thickness and moist-bulk-density values.

According to Pack et al. (1998b, 2005), the T/R ratio multiplied with the sine of the slope angle can be interpreted as the length of hillslope required to develop saturation in a critical wet period. Although the term 'steady state' is used with lateral flux (Section 2.2), the parameter R does not refer to a long-term (e.g., annual) average of recharge in SINMAP. Instead it represents the effective recharge for a critical period or event of wet weather that is likely to trigger landslides.

The T/R ratio, which is treated as a single parameter, combines both climate and hydrogeological factors. The effective R value can be defined as rainfall minus evapotranspiration and infiltration. Evapotranspiration and infiltration are assumed as negligible in this study. Such an assumption represents a worst-case scenario by overestimating the value of R. However it is generally acceptable for heavy storms of short duration.

As mentioned earlier, previous studies of landslides and associated debris flows on several landslide sites on Oahu reveal that shallow landslides are activated by extreme and intense rainfall events (Torikai

Table 4
Initial setting of SINMAP modeling hydrological and geotechnical parameter values for different watersheds of each region of the multi-region calibration theme.

Region	Watershed	Soil depth [m]	Moist bulk density [kg m^{-3}]	K_s min. [m day^{-1}]	K_s max. [m day^{-1}]	C min.	C max.	T min. [m^2 day^{-1}]	T max. [m^2 day^{-1}]	T/R min. [m]	T/R max. [m]
1	Kalihi	1.78	1400	0.366	3.658	0	0.983	0.650	6.503	1.885	18.850
	Nuuanu	1.78	1400	0.366	3.658	0	0.983	0.650	6.503	1.885	18.850
	Kapalama	1.78	1400	0.366	3.658	0	0.983	0.650	6.503	1.885	18.850
	Manoa-Palolo	1.83	1300	1.219	3.658	0	1.029	2.230	6.689	6.463	19.388
	Makiki	1.78	1100	1.219	3.658	0	1.251	2.168	6.503	6.283	18.850
	Ala Wai	1.83	1600	0.366	12.192	0	0.836	0.669	22.297	1.939	64.628
	Waialaenui	1.83	1560	0.061	12.192	0	0.858	0.111	22.297	0.323	64.628
	Diamond Head	1.78	1400	0.061	1.219	0	0.983	0.108	2.168	0.314	6.283
2	Waimanalo	1.93	1600	0.366	12.192	0	0.792	0.706	23.535	2.469	82.292
	Kahawai	1.78	1300	0.366	12.192	0	1.058	0.650	21.677	2.274	75.795
	Wailupe	1.93	1400	0.366	3.658	0	0.905	0.706	7.061	2.469	24.688
	Makapuu	1.83	1400	0.366	3.658	0	0.956	0.669	6.689	2.339	23.388
	Kuliouou	1.78	1560	0.366	3.658	0	0.882	0.650	6.503	2.274	22.739
	Niu	1.83	1560	1.219	3.658	0	0.858	2.230	6.689	7.796	23.388
	Kamiloiki	1.78	1560	0.366	3.658	0	0.882	0.650	6.503	2.274	22.739
	Kamilo Nui	1.78	1400	0.061	3.658	0	0.983	0.108	6.503	0.379	22.739
	Koko Crater	1.52	1600	0.366	12.192	0	1.003	0.557	18.581	1.949	64.967
	Portlock	1.78	1600	0.366	12.192	0	0.860	0.650	21.677	2.274	75.795
	Hanauma	1.52	1400	0.366	3.658	0	1.147	0.557	5.574	1.949	19.490
3	Keaahala	1.78	1200	1.219	3.658	0	1.147	2.168	6.503	7.178	21.534
	Puu Hawaiiloa	1.83	1400	1.219	3.658	0	0.956	2.230	6.689	7.383	22.149
	Kaneohe	1.78	1300	1.219	3.658	0	1.058	2.168	6.503	7.178	21.534
	Kawa	1.65	1400	0.366	3.658	0	1.058	0.604	6.039	2.000	19.996
	Kaelepulu	1.93	1600	1.219	12.192	0	0.792	2.354	23.535	7.793	77.932
	Kawainui	1.93	1600	0.061	12.192	0	0.792	0.110	21.946	0.363	72.668
4	Kalauao	1.78	1450	0.366	3.658	0	0.949	0.650	6.503	2.970	29.695
	Halawa	1.78	1400	0.366	3.658	0	0.983	0.650	6.503	2.970	29.695
	Aiea	1.78	1400	0.061	3.658	0	0.983	0.108	6.503	0.495	29.695
	Moanalua	1.78	1400	0.366	3.658	0	0.983	0.650	6.503	2.970	29.695
	Salt Lake	1.22	1400	0.366	1.219	0	1.433	0.446	1.486	2.036	6.787
	Keehi	1.78	1400	0.061	1.219	0	0.983	0.108	2.168	0.495	9.898
	Manuwai	1.78	1400	0.061	1.219	0	0.983	0.108	2.168	0.495	9.898

and Wilson, 1992; Wilson et al., 1992; Peterson et al., 1993; Ellen et al., 1991, 1993, 1995). However, there is no consensus on the rainfall threshold that determines the triggering of shallow landslides in the study area. Historical severe rainfall records examined against debris-flow occurrences suggest that the intensities of non-landslide-producing rainfall events do not significantly differ from landslide producing extreme events within each region. Hence, it is difficult to derive any significant envelope for defining the threshold rainfall rate that is likely to trigger shallow landslides within each region. We used in our calculations a quasi-dynamic scenario of soil wetness and slope-stability index based on daily rainfall events with return periods of years.

Nearly 90-year-long daily rainfall record from 1919 to 2007 was used to determine rainfall magnitude and frequency relationships for each calibration region. The data were obtained from 26 USGS and NOAA NWS raingauge stations in the study area (Fig. 2). Selected raingauge stations either recorded rainfall hourly or had continuous records from which hourly or daily readings could be computed. Daily rainfall values for various return periods were fitted with a Log Pearson type III distribution. Fig. 4 shows daily rainfall and frequency (return period) curves for each region of the study area. The corresponding rainfall for a certain return period can be estimated from the fitted value distribution which represents an estimate of the maximum-daily-rainfall event that is likely to occur in such a time span. This expected maximum rainfall rate was assumed as the trigger of shallow landslides and was used to calculate the upper and lower boundary values for the T/R ratio.

For each region a series of model predictions were initially evaluated using values of T/R based on different daily rainfalls for return periods of 10, 25, 50, and 100 years. However, these preliminary results suggested that values of T/R calculated with daily rainfall values for return periods of 50 and 100 years performed better in identifying 100% of the total landslide inventory. There were also negligible differences in model predictions between the return period of 50 and 100 years. Hence, the values of T/R calculated using the rainfall values for a return period of 50 years were used for the analysis (Table 4).

3.2.4. Geotechnical data

The cohesion index (dimensionless cohesion factor C) and the soils internal friction angle (ϕ) represent the geotechnical data input into the model. C is the relative contribution of soil and root cohesive forces in preventing the development of a failure plane (defined in Eq. (2)). Although the SSURGO database lists the Atterberg limits (e.g., liquid limit, plastic limit, and plasticity index) of soils for each calibration region, the values of soil cohesion (C_s) are not available for most of the soils within the calibration regions. However, soil geotechnical data for critical landslide-prone areas of regions 1, 2, and 3 are reported by Ellen et al. (1995).

Baum et al. (1990, 1991) tested geotechnical properties for a range of landslide soils in Manoa Valley. They found that the matrix material had high plasticity and low-to-moderate residual shear strength (plastic limits and liquid limits ranged from 29 to 61 and from 59 to 137, respectively). The matrix contained roughly 50–80% clay, 10–30% silt, and 5–25% sand. Soils that were clay rich with high liquid limits (from about 95 to 137) had low strengths characterized by friction angles from 6° to 11° and cohesion values from 0 to 10.5 kN m^{-2}. Samples having relatively low liquid limits (from about 59 to 75) generally had higher residual strengths, characterized by friction angles ranging from 20° to 25° and cohesion values ranging from 7 to 11 kN m^{-2}.

Ellen et al. (1995) provided values of the Atterberg limits, geotechnical properties of landslide soils, and their relation with the Atterberg limits in the areas extending from Moanalua Valley to the north to Kamilo Nui Valley to the east of the Honolulu District. Recently Kaya and Kwong (2007) studied geotechnical properties of Hawaiian landslide soils. They observed that the residual friction angles of landslide soils ranged from 5.5° to 19° with a mean of 11.6° and the cohesion ranged from 0 to 6 kN m^{-2} with an average of 0.5 kN m^{-2}. The friction angle of soil samples taken from the upper layer of colluvial deposits ranged from 6.9° to 29.3° with a mean of 21.4° and cohesion ranged from 0 to 64 kN m^{-2} with a mean of 21 kN m^{-2}.

To avoid the complication of variable landslide parameters in a regional analysis and to isolate the topographic control on landslide initiation, we used uniform parameter values of friction angle and cohesion of the soil for all watersheds in the study area. The values of friction angle and cohesion of the soil derived from previous studies varied from 5° to 40° and 0 to 21 kN m^{-2}, respectively.

Field observations of soil exposed at the head scarp of landslides reveal that tree roots do not penetrate into the weathered rock (Ellen et al., 1993; 1995; Peterson et al., 1993), and consequently the root zone is situated above the failure plane. Based on the soil-root morphology nomenclature suggested by Tsukamoto and Kusakabe (1984), these conditions are referred to as Type A, which have the root strength (C_r) probability distributions defined by a mean value of 3 kN m^{-2} and standard deviation of 2 kN m^{-2}. We considered values for the root cohesive force (C_r) of 0–3 kN m^{-2} and for soil cohesive force (C_s) of 0–21 kN m^{-2}. Such values provided lower and upper boundary values of the cohesion index (C) of 0–1.4 (Table 4). A series of SINMAP calculations in which the values of C varied and all other parameters remained unchanged showed the significant influence of such a parameter on slope-stability calculations in all regions. For each calibration region we initially evaluated a range of values of 5°–40° for friction angles of soils and values of 0–1.4 for dimensionless cohesion. Finally we selected calibrated lower and upper boundary values of 10° and 40°, and 0 and 0.65 for friction angle of soils and dimensionless cohesion, respectively. These calibrated values were used in the SINMAP application for all calibration regions.

4. Results and discussion

Spatial variability of input parameters was defined in this study by a careful selection of locations which were representative of each region. Parameter uncertainty was simplified with the use of uniform probability distributions with upper and lower boundaries of parameters. As mentioned earlier, the representative upper and lower boundary values of friction angle and the combined cohesion index were considered constant and uniformly distributed over the entire study domain with or without shallow landslides.

SINMAP is calibrated by comparing simulation results against inventoried landslide initiation points. The values of T/R parameters, which are difficult to measure, were adjusted to improve model prediction. Results of calibration showed that there was negligible difference between using the upper and lower values of friction-angle values (10° and 40°). Morrissey et al. (2001) also observed that changing values of friction-angle within a specified range showed only minor changes in SINMAP's results. Therefore, failure is likely more sensitive to other factors such as slope and the cohesion index. According to Hammond et al. (1992), the cohesion index increases with decreasing soil depth. A sensitivity analysis of the role of the parameter C was carried out assuming that plant roots can be influential. Results from a series of calculations in which dimensionless cohesion varied (0–1.4) and all other parameters remaining unchanged revealed that C had a significant influence on the stability calculations. The calibrated value of C covered a range between 0 and 0.65, which represents a cohesion value between 0 and 11.2 kN m^{-2}. This relatively lower range of cohesion values may suggest that colluvium, residual soils, or completely weathered materials in the study area are clay rich and possess low strengths (Baum et al., 1990, 1991; Kaya and Kwong, 2007). The value of 0 for the lower bound of C may imply drained conditions during the failure of the landslides, as suggested by Guzzetti et al. (1996).

Table 2 lists classes of slope stability based on *SI* values as set by SINMAP. The upper and lower thresholds characterize regions where the probability of failure is greater than or less than 50%, respectively. Stable, moderately stable, and quasi-stable are used to classify regions that should not fail with the most conservative values of the specified parameter ranges. The defended-slope classification is used to characterize regions where the slope should be unstable for any values within parameter ranges, i.e., the probability of failure with the specified range of parameters is the greatest.

The *SI* distribution maps of calibration regions 1, 2, 3, and 4 are shown in Figs. 5–8, respectively. The SINMAP approach to instability modeling successfully located all 226 observed shallow landslides within areas classified as unstable. The largest number of landslides is found in the lower-threshold stability class that represents 21% of the area (high landslide susceptibility), while upper-threshold stability class includes 18% of the study area (very high susceptibility). About 55% of the study area is classified with *SI* below one (upper- and lower-threshold classes) or equal to zero (defended class), characterizing highly unstable conditions. About 34% of the area is stable while 11% is moderately stable or quasi-stable, indicating that minor destabilizing factors could lead to instability for these low-to-medium susceptible areas.

Various regions show contrasting results, reflecting influences of different instability mechanisms (Figs. 5–8). The percentage of areas classified as unstable were about 71%, 53%, 49%, and 66%, for regions 1 through 4, respectively. For region 1 the defended class covers the largest percentage of the total area (about 31%). Lower-threshold, upper-threshold, and stable classes cover 15%, 13%, and 25% of that region, respectively. In contrast, only about 5% of the area for region 2, 9% for the region 3, and 12% for region 4 are predicted as the defended class.

The largest area percentages (43%, 35%, and 34%, respectively) fall within the stable class for these regions. The upper- and lower-threshold classes represent about 18% and 24% for region 2, 14% and 20% for region 3, and 28% and 26% for region 4, respectively.

Of significant note, SINMAP failed to predict areas classified as moderately stable or quasi-stable in region 4. The excessive prediction of highly susceptible areas may be attributed to the fact that, in model calibration, we attempted to adjust parameters in identifying most of the inventoried landslides in areas referred to as unstable. This parameter adjustment may have effectively reduced the areas classified as low-to-medium susceptibility.

For regions 1 to 4, Fig. 9 illustrates the distribution of contributing areas within different stability indices, in plots defined in terms of slope and specific catchment area (Pack et al., 1998b, 2005). In Fig. 9 the inventoried landslides are plotted based on the values of the surface slope and specific catchment area of the cell in which each landslide point is located. Lines of stability index (vertical lines) define the boundaries for regions within slope-specific catchment areas that have similar potentials for stability or instability (as listed in Table 2). Considering a lower wetness threshold of 10% (as suggested by Pack et al., 1998b, 2005), saturation-region lines (near-horizontal curved lines) provide boundaries for regions having similar wetness potentials within slope-specific catchment areas.

The total numbers of slides are 88, 85, and 45 for regions 1, 2, and 3, respectively. Of these, 81, 53, and 45, respectively, fall within the lowest four stability classes (Fig. 9a–c). For region 1 the largest number of landslides falls within the defended class (30). In contrast, regions 2 and 3 include large numbers (27 and 17, respectively) of landslides in areas within the lower-threshold class. For region 4 three-fourths (6 out of 8) of the landslides are from lower- to upper-threshold slopes and no landslides fall within the defended class (Fig. 9d).

Except for region 3, model results were not accurate by locating a number of landslides within areas predicted as stable. These errors are generally related to slope modifications not represented in the available data. Such modifications include land-use practices that reduced the stabilizing forces in slopes in presumably stable areas, leading to landslides. For example, in addition to dominant scrub/shrub and evergreen forest land covers (C-CAP), regions 1, 2, and 4 comprise a total of 42%, 24%, and 39%, respectively, of the region's areas for both

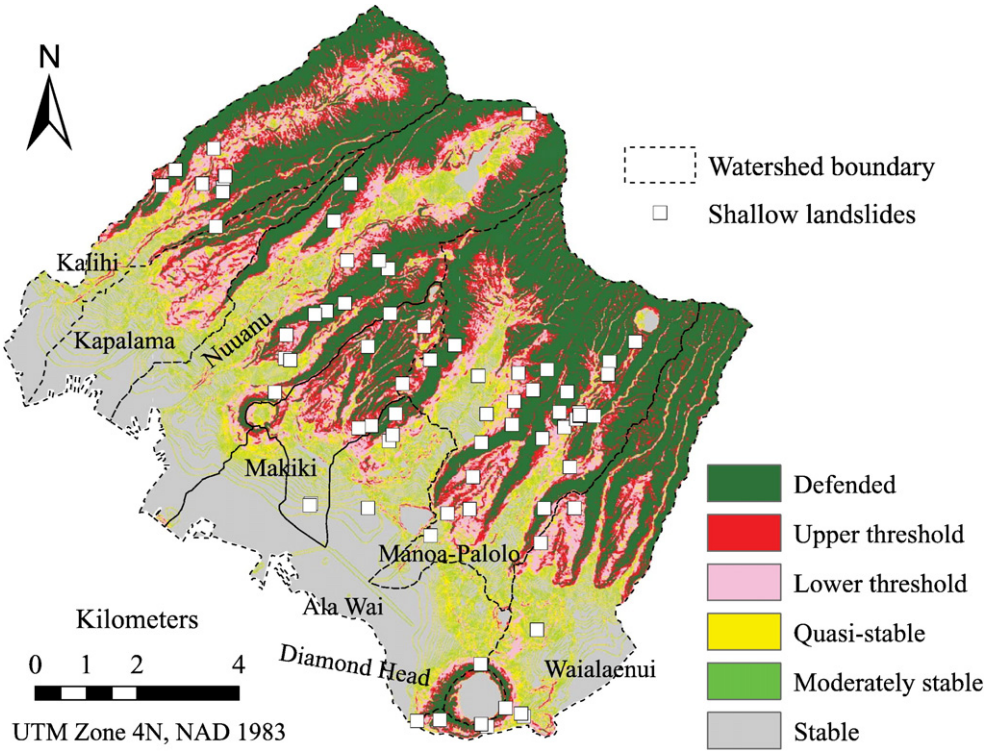

Fig. 5. Slope-stability index distribution for calibration region 1.

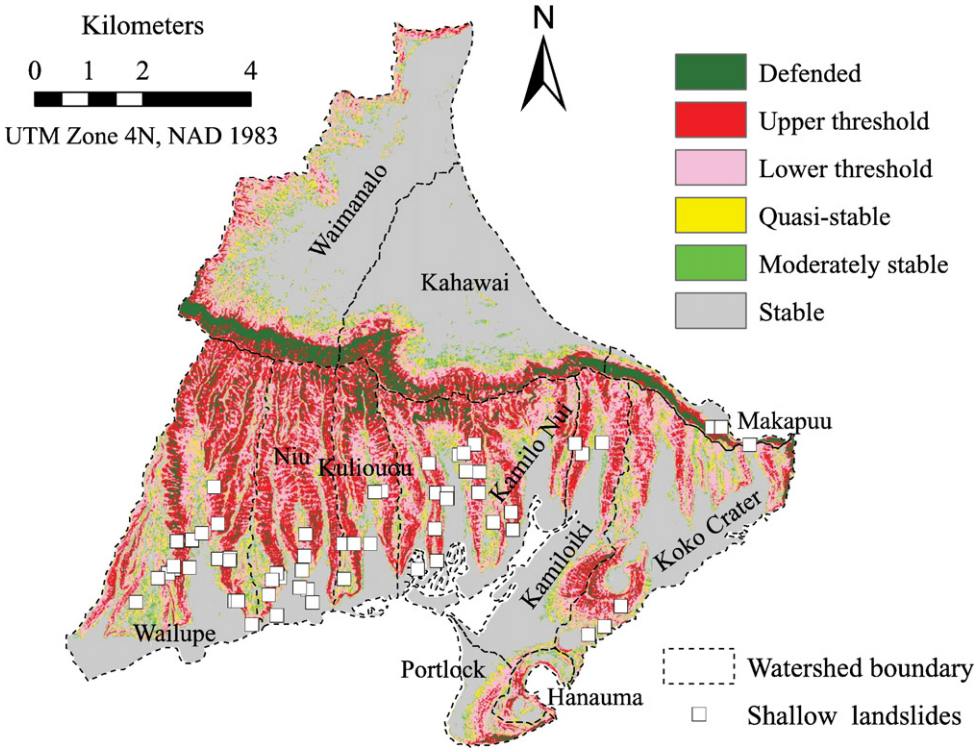

Fig. 6. Slope-stability index distribution for calibration region 2.

low- and high-intensity developed land covers (Table 1). Impervious surfaces account for 21% to 49% and 80% to 100% of total cover, for low- and high-intensity developed land covers, respectively. The SINMAP model is not able to account for the effects of such significant areas of impervious surface cover.

Fig. 10 shows the SINMAP-prediction summary for calibration regions 1, 2, 3, and 4. Contrasting results prevail among different regions. The total value of landslide densities are 0.8, 1.04, 0.54, and 0.07 landslides per km^2, respectively, for regions 1 to 4. It should be kept in mind that the landslide density for region 4 is based on an

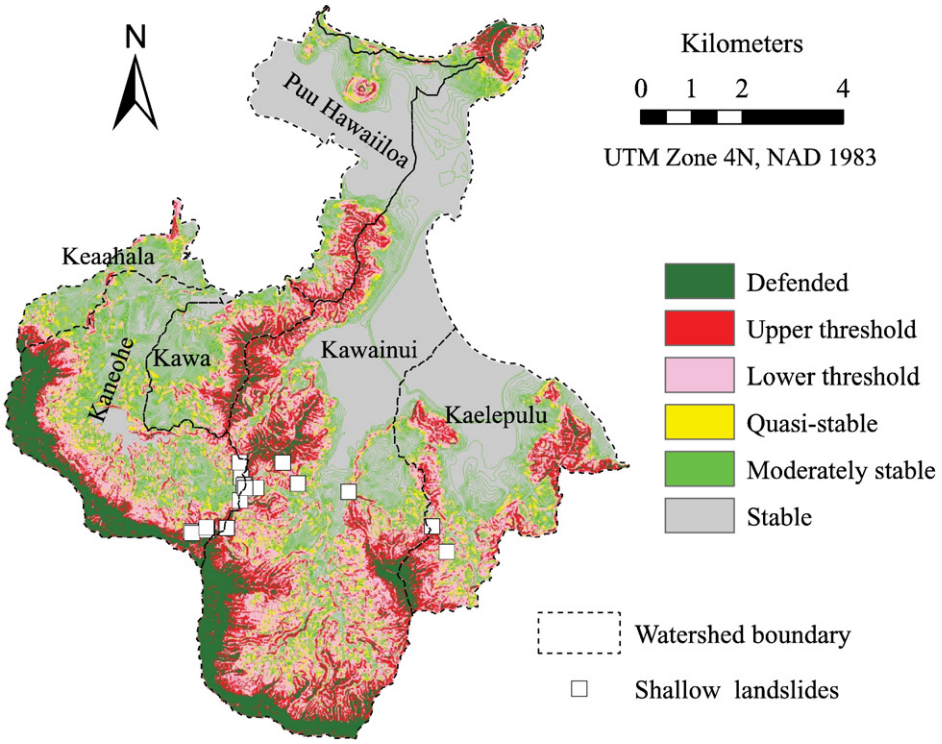

Fig. 7. Slope-stability index distribution for calibration region 3.

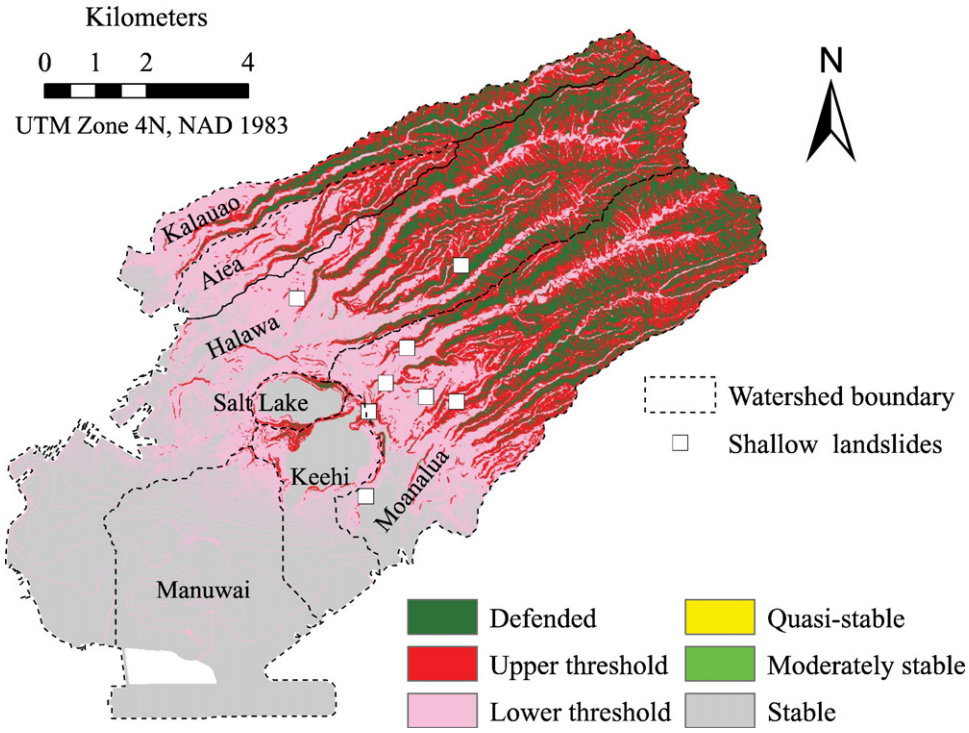

Fig. 8. Slope-stability index distribution for calibration region 4.

incomplete and most likely non-representative landslide inventory. As mentioned earlier (Section 3.2.1), information on historical landslide events was compiled from different sources that have few explanations concerning the exact initiation location of the landslides. Very few (eight) shallow landslides were inventoried for region 4 mostly on residential or developed areas, in which the accounts are much more frequent.

The defended class has the highest density of 0.3 landslides per km^2 in region 1. On the other hand, region 2 has the highest density of 0.33 landslides per km^2 in areas predicted as lower-threshold stability

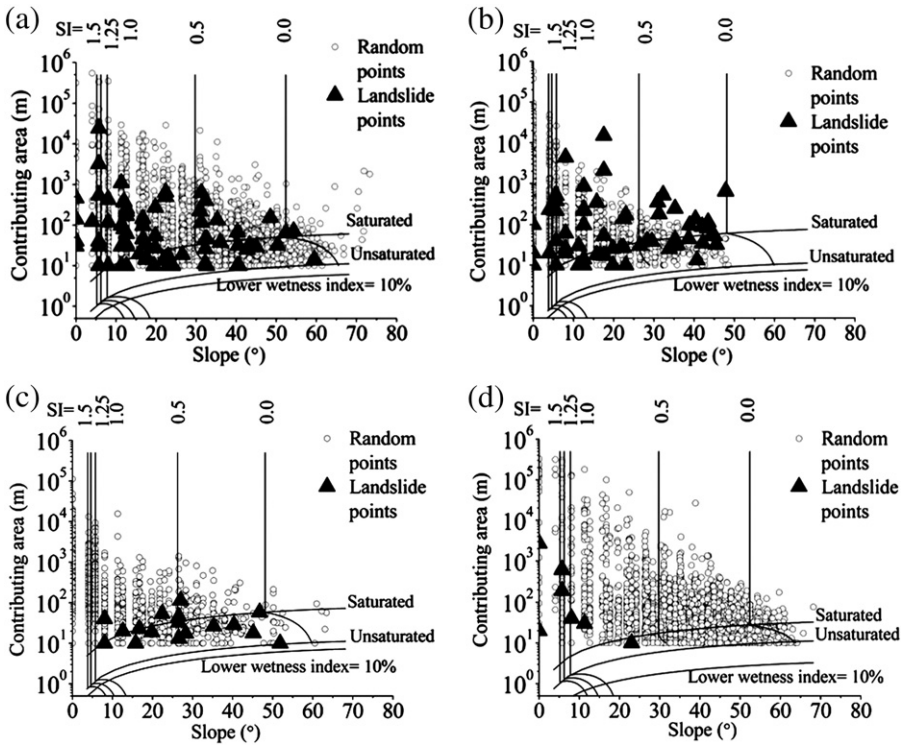

Fig. 9. Plot showing the relationship between catchment area and the ground-surface slope calculated at grid cell points and inventoried landslides for regions 1 to 4 (a to d). Stability index region lines (vertical lines) define boundaries for regions within slope-specific catchment area space that have similar potential for stability or instability, as listed in Table 2. Saturation region lines (near-horizontal curved lines) provide boundaries for regions within slope-specific area space that have similar wetness potential.

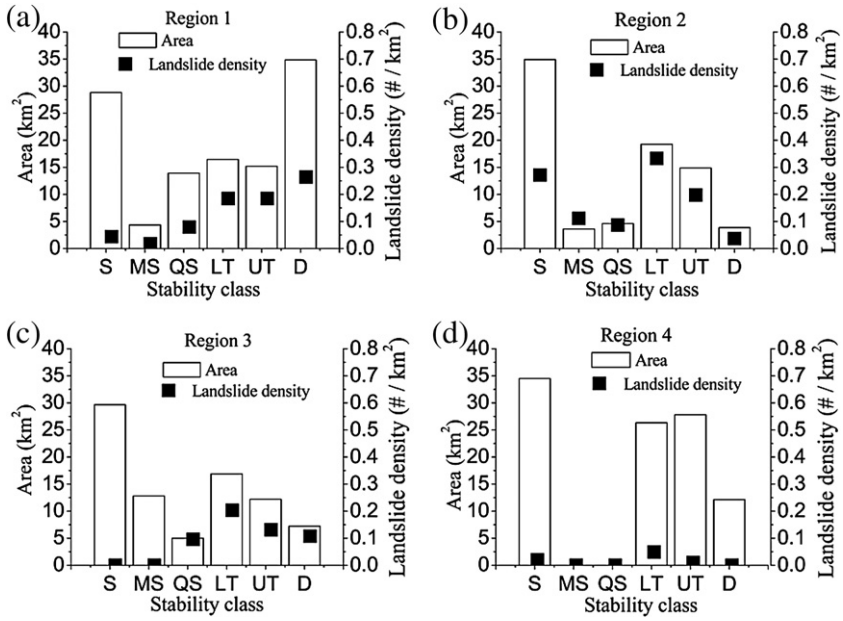

Fig. 10. Summary of the SINMAP model (square = landslide density, bars = area of the stability class; S: stable, MS: moderately stable, QS: quasi-stable, LT: lower threshold, UT: upper threshold, and D: defended) for calibration regions.

class. Both regions 1 and 2 possess the highest landslide density of 0.2 landslides per km^2 in areas identified as the upper-threshold class.

Lower landslide density is predicted in region 4, (representing southern leeward Oahu) in comparison to most of the watersheds in regions 1, 2, and 3 (which fall within eastern and southeastern windward Oahu) that receive more frequent extreme rainfalls (Fig. 4). For regions 1, 2, and 3, the areas falling in unstable classes increase with the relatively higher expected extreme rainfalls, with a decrease in areas falling in stable classes. A relatively high landslide density of 0.3 landslides per km^2 is predicted for region 2. However, the model results are inaccurate considering that the highest landslide density falls in areas classified as stable.

For additional validation for areas underlain by Koolau Basalt (which covers most of the Honolulu District—Stearns, 1939; Langenheim and Clague, 1987) slope-stability index maps were compared against the debris-flow hazard maps developed by Ellen et al. (1993). SINMAP predicts the areas where debris-flow may originate, but not their magnitude, runout or depositional areas. Therefore, stability indices predicted by the model should be interpreted in terms of relative hazard. Although direct comparison between the slope-stability maps and the debris-flow hazard maps is not possible, association was made for regions 1, 2, and 4. As shown in Table 1, Ellen et al. (1993) classified areas as low, moderate, or high susceptibility based on the relative degree of hazard from hillslope debris flows. These three classes are based on an average size and travel-distance behavior of debris flows for return periods of 2001 to 10,000 years, 501 to 2000 years, and 500 years or less, respectively.

The steep terrain along the Koolau Range, delineated by Ellen et al. (1993) as moderate-to-high hazard for region 1 and low-to-moderate hazard for regions 2 and 4, respectively, are mostly predicted as unstable by SINMAP. High debris-flow hazard is common in steep drainage areas but is rare for roads or in suburban valley areas along the Koolau Range. Such areas are successfully defined as being in the defended class by SINMAP.

Moderate and low hazards occur on hillslopes and in places extending into and in suburban valley margins of the study area, respectively. SINMAP predicted lower- and upper-threshold-stability-index distributions in these areas. As shown in Figs. 2 and 5–8, terrain predicted by SINMAP as defended, lower-, and upper-threshold-stability are typically found where shallow landslides are triggered on 20°–82° slopes. Table 1 shows that regions 1, 2, and 4 are significantly composed of such terrain, covering, respectively, 49%, 38%, and 43% of the regions.

Finally, most of the study areas where shallow landslides are triggered, according to SINMAP, are composed of clayey soils. The susceptibility to landslides in relation to the geotechnical properties of ultisols and vertisols soils has been discussed in several studies including De Silva (1974), Jellinger (1977), Baum et al. (1990), Ellen et al. (1995), and Kaya and Kwong (2007).

It is important to state that, although most watersheds of calibration regions 1, 2, and 4 are identified as susceptible to shallow landslides or debris slides, instability may arise simply due to a combination of parameter values within the upper and lower boundaries. In the defended class, regions are characterized such that the slope should be unstable for any parameter combination within the given parameter ranges. The model can be inappropriate in some cases where such slopes occur, as in the case of bare slopes or slopes devoid of soil cover along the Koolau Range.

5. Conclusions

The deterministic slope-stability model SINMAP was applied to assess the susceptibility of slopes to shallow landslides in 32 watersheds of eastern to southern areas of Oahu, Hawaii, under daily rainfall events with a return period of 50 years. The study area of about 384 km^2 was divided into four calibration regions with different geotechnical and hydrological characteristics. The shallow landslide susceptibility of each region was assessed by comparing slope-stability-index maps of susceptible areas, produced by the model, with inventoried landslides and previous susceptibility appraisals.

The model assessed susceptibility at all 226 inventoried shallow landslide locations, and classified these susceptible areas as unstable. About 55% of the study area is classified as defended, lower-, or upper-threshold stability classes, which refer to conditions that are highly unstable and thus critical. About 34% of the study area is classified as stable (safe), while 11% of the area is classified as moderately stable and quasi-stable zones, suggesting low-to-medium susceptibility levels. Calibration regions show contrasting results; the percentage of areas classified as unstable were about 71%, 53%, 49%, and 66% for regions 1 to 4, respectively.

For qualitative validation, the slope-stability-index maps produced by SINMAP were compared with the debris-flow-hazard maps of Ellen et al. (1993) for the assessment of predicted shallow-landslide susceptibility and potential debris-flow damage in regions 1, 2, and 4. The comparison indicates that steep terrain with clayey soils, classified as low-to-moderate and moderate-to-high debris-flow susceptibility by Ellen et al. (1993), was also predicted as unstable by SINMAP. Therefore, it is reasonable to assume that the SINMAP model can be utilized as a tool for identification of both hazardous and safe shallow-landslide zones in the study area. However, slope-stability-index distributions predicted by this study should be complemented with additional detailed geotechnical investigations of susceptible areas.

Mitigation measures should be taken and land-use restrictions should be imposed to minimize the landslide risk in areas delineated as defended, lower-, and upper-threshold instability. Areas identified as low-to-medium susceptibility level (quasi-stable or moderately stable) should only be developed after conducting more detailed stability appraisals and applying land-use regulations and well-engineered construction practices. No additional regulations should be required for areas identified as stable.

It can be concluded that SINMAP is generally applicable to Hawaii and similar young volcanic environments with watersheds characterized by steep terrain, abundant moisture supply, and heavy annual rainfalls. Shallow-landslide assessment presented in this study would be particularly useful for the tropics, considering that most tropical regions are in developing countries where data are either uncertain, incomplete, or even absent. In most cases, hydrologic monitoring is scarce due to limited resources, and research mostly relies on aerial photo interpretation, field observation, and soil or material testing.

Model limitations are primarily related to data availability. SINMAP provides a general depiction of shallow landslide susceptibility across the study area; however, the model cannot be used to predict failure size, mobility, or consequences. SINMAP predictions may be further improved by incorporating heterogeneous and anisotropic soil properties and spatial and temporal variations of rainfall. Additionally, model resolution may be enhanced by improving the accuracy of the DEM by using higher-resolution data (e.g., Interferometric Synthetic Aperture Radar [IfSAR/InSAR] DEMs) and increasing the accuracy of the mapped locations of landslide initiations. Stability-index-distribution maps would be useful for any studies attempting to delineate susceptible areas of debris-flow production and attempting to assess such flows. Predicted slope-stability data will aid in explaining causes of known landslides, making emergency decisions, and, ultimately, significantly mitigating future landslide risks.

Acknowledgments

This paper is published as a part of the continuing University of Hawaii at Manoa Water Resources Research Center “Contributed Papers” series. As such it will be assigned a sequential “WRRC-CP” number upon publication and this number, along with the abstract of the paper, will then be posted at the WRRC website <http://www.wrrc.hawaii.edu/index.html>. Constructive comments and helpful suggestions from Francisco Gutierrez and an anonymous reviewer substantially improved the manuscript and are gratefully acknowledged.

References

Baum, R.L., Reid, M.E., 1992. Geology, hydrology and mechanics of the Alani-Paty landslide, Manoa Valley, Oahu, Hawaii. Open File Report. U.S. Geological Survey, pp. 92–501.

Baum, R.L., Fleming, R.W., Ellen, S.D., 1989. Maps showing landslide features and related ground deformation in the Woodlawn area of the Manoa Valley, City and County of Honolulu, Hawaii. Open File Report. U.S. Geological Survey, pp. 89–290.

Baum, R.L., Spengler, S.R., Torikai, J.D., Liu, L.A., 1990. Summary of geotechnical and hydrologic data collected through April 30, 1990, for the Alani-Paty landslide, Manoa Valley, Honolulu, Hawaii. Open File Report. U.S. Geological Survey, pp. 90–531.

Baum, R.L., Reid, M.E., Wilburn, C.A., Torikai, J.D., 1991. Summary of geotechnical and hydrologic data collected from May 1, 1990 through April 30, 1991, for the Alani-Paty landslide, Manoa Valley, Honolulu, Hawaii. Open File Report. U.S. Geological Survey, pp. 91–598.

Beven, K.J., Kirkby, M.J., 1979. A physically based variable contributing area model of basin hydrology. Hydrological Sciences Bulletin 24, 43–69.

Calcaterra, D., de Riso, R., Di Martire, D., 2004. Assessing shallow debris slide hazard in the Agnano Plain (Naples, Italy) using SINMAP, a physically based slope-stability model. In: Lacerda, W.A., Ehrlich, M.E., Fontoura, S.A.B., Sayao, A.S.F. (Eds.), Taylor and Francis Group, London, pp. 177–183. vol. 1.

Campbell, R.H., 1975. Soil slips, debris flows, and rainstorms in the Santa Monica Mountains and vicinity, Southern California. U.S. Geological Survey, Professional Paper, vol. 851.

Carson, H.L., Clague, D.A., 1995. Geology and biogeography of the Hawaiian Islands. In: Wagner, W.L., Funk, V.A. (Eds.), Hawaiian Biogeography: Evolution on a Hot Spot Archipelago. Smithsonian Institution Press, Washington D.C., pp. 14–29.

Casadei, M., Dietrich, W.E., Miller, N.L., 2003. Testing a model for predicting the timing and location of shallow landslide initiation in soil-mantled landscapes. Earth Surface Processes and Landforms 28, 925–950.

Cruden, D.M., Varnes, D.J., 1996. Landslide types and processes. In: Turner, A.K., Schuster, R.L. (Eds.), Landslides: Investigation and Mitigation, Special Report, vol. 247. Transportation Research Board, National Research Council, Washington, DC, pp. 36–75.

De Silva, G.L.R., 1974. Slope stability problems induced by human modification of the soil covered hillslopes of Oahu, Hawaii. Ph.D. Dissertation, University of Hawaii, Honolulu, Hawaii, USA.

Dietrich, W.E., Wilson, C.J., Montgomery, D.R., McKean, J., Bauer, R., 1992. Erosion thresholds and land surface morphology. Geology 20, 675–679.

Dietrich, W.E., Wilson, C.J., Montgomery, D.R., McKean, J., 1993. Analysis of erosion thresholds, channel networks, and landscape morphology using a digital terrain model. Journal of Geology 101, 259–278.

Dietrich, W.E., Reiss, R., Hsu, M., Montgomery, D.R., 1995. A process-based model for colluvial soil depth and shallow land sliding using digital elevation data. Hydrological Processes 9, 383–400.

Dietrich, W.E., Bellugi, D., Real De Asua, R., 2001. Validation of shallow landslide model, SHALTAB, for forest management. In: Wigmosta, M.S., Burges, S.J. (Eds.), Land Use and Watersheds: Human Influence on Hydrology and Geomorphology in Urban and Forest Areas. Water Science and Application Series, vol. 2. American Geophysical Union, pp. 195–227.

Dracup, J.A., Cheng, E.D.H., Nigg, J.M., Schroeder, T.A., 1991. The New Year's Eve Flood on Oahu, Hawaii, December 31, 1987–January 1, 1988. Natural Disaster Studies, vol. 1. National Research Council. 72 pp.

Ellen, S.D., Wieczorek, G.F., 1988. Landslides, floods, and marine effects of the storm of January 3–5, 1982, in the San Francisco Bay region, California. Professional Paper, vol. 1434. U.S. Geological Survey.

Ellen, S.D., Iverson, R.M., Pierson, T.C., 1991. Map showing the distribution of debris flows during the New Year's Eve storm of 1987–1988 in southeastern Oahu, Hawaii. Open File Report. U.S. Geological Survey, pp. 91–129.

Ellen, S.D., Mark, R.K., Cannon, S.H., Knifong, D.L., 1993. Map of debris-flow hazard in the Honolulu District of Oahu, Hawaii. Open File Report. U.S. Geological Survey, pp. 93–213.

Ellen, S.D., Liu, L.S.M., Fleming, R.W., Reid, M.E., Johnsson, M.J., 1995. Relation of slow-moving landslides on earth materials and other factors in valleys of the Honolulu District of Oahu, Hawaii. Open File Report. U.S. Geological Survey, pp. 95–218.

Federal Emergency Management Agency (FEMA), 1988. Interagency Flood Hazard Mitigation Report in Response to the January 8, 1988 Disaster Declaration (FEMA-808-DR-HI)/prepared by the FEMA Region IX Interagency Flood Hazard Mitigation Team, Washington, DC. 34 pp.

Giambelluca, T.W., Nullet, M.A., Schroeder, T.A., 1986. Rainfall Atlas of Hawaii. State of Hawaii, Department of Land and Natural Resources, Division of Water and Land Development, Report R76. 267 pp.

Grayson, R.B., Moore, I.D., McMahon, T.A., 1992a. Physically based hydrologic modeling 1. A terrain-based model for investigative purposes. Water Resources Research 28, 2639–2658.

Grayson, R.B., Moore, I.D., McMahon, T.A., 1992b. Physically based hydrologic modeling 2. Is the concept realistic. Water Resources Research 28, 2659–2666.

Guzzetti, F., Cardinali, M., Rei, chen bach, P., 1996. The influence of structural settings and lithology on landslide type and pattern. Environmental and Engineering Geoscience 2, 531–555.

Hammond, C., Hall, D., Miller, S., Swetik, P., 1992. Level I Stability Analysis (LISA) documentation for version 2.0. USDA Forest Service Intermountain Research Station, General Technical Report INT-285.

Hill, B.R., Fuller, C.C., Decarlo, E.H., 1997. Hillslope soil erosion estimated from aerosol concentrations, North Halawa Valley, Oahu, Hawaii. Geomorphology 20, 67–79.

Jellinger, M., 1977. Methods of detection and analysis of slope instability, southeast Oahu, Hawaii. Ph.D. Dissertation, University of Hawaii, Honolulu, Hawaii, USA.

Johnsson, M.J., Ellen, S.D., McKittrick, M.A., 1993. Intensity and duration of chemical weathering: and example from soil clays of the southeastern Koolau Mountains, Oahu, Hawaii. In: Johnsson, M.J., Basu, A. (Eds.), Processes Controlling the Composition of Clastic Sediments. Special Paper, vol. 284. Geological Society of America, pp. 147–170.

Kaya, A., Kwong, J.K.P., 2007. Evaluation of common practice empirical procedures for residual friction angle of soils: Hawaiian amorphous material rich colluvial soil case study. Engineering Geology 92, 49–58.

Kwong, J., Spengler, S., Wang, N., Wan, A., 1999. Some important engineering geological and hydrological factors influencing slope stability in Hong Kong and Hawaii. In: Clarke, B. (Ed.), Urban Ground Engineering. Thomas Telford, London, pp. 235–252.
Langenheim, V.A.M., Clague, D.A., 1987. The Hawaiian-Emperor volcanic chain, Part 2, Stratigraphic framework of volcanic rocks of the Hawaiian Islands. In: Decker, R.W., Wright, T.L., Stauffer, P.H. (Eds.), Volcanism in Hawaii. Professional Paper, vol. 1350. U.S. Geological Survey, pp. 55–84.
Lan, H.X., Zhou, C.H., Wang, L.J., Zhang, H.Y., Li, R.H., 2004. Landslide hazard spatial analysis and prediction using GIS in the Xiaojiang watershed, Yunnan, China. Engineering Geology 76, 109–128.
Li, Y.-H., 1988. Denudation rates of the Hawaiian Islands by rivers and groundwaters. Pacific Science 42, 253–266.
Macdonald, G.A., Abbott, A.T., Peterson, F.L., 1983. Volcanoes in the Sea, the Geology of Hawaii, 2nd ed. University of Hawaii Press, Honolulu. 517 pp.
Meisina, C., Scarabelli, S., 2007. A comparative analysis of terrain stability models for predicting shallow landslides in colluvial soils. Geomorphology 87, 207–223.
Montgomery, D.R., Dietrich, W.E., 1994. A physically based model for the topographic control on shallow landsliding. Water Resources Research 30, 1153–1171.
Montgomery, D.R., Schmidt, K.M., Green Berg, H.M., Dietrich, W.E., 2000. Forest cleaning and regional landsliding. Geology 28, 311–314.
Moore, J.G., Mark, R.K., 1992. Morphology of the island of Hawaii. GSA Today 2, 1–7.
Morrissey, M.M., Wieczorek, G.F., Morgan, B.A., 2001. A comparative analysis of hazard models for predicting debris flows in Madison County, Virginia. Open File Report 01-0067. U.S. Geological Survey.
NOAA, 2000. Main Eight Hawaiian Islands Cover. National Oceanic and Atmospheric Administration, Coastal Services Center, South Carolina, USA.
O'Loughlin, E.M., 1986. Prediction of surface saturation zones in natural catchments by topographic analysis. Water Resources Research 22, 794–804.
Pack, R.T., Tarboton, D.G., Goodwin, C.N., 1998a. In: Moore, D.P., Hungr, O. (Eds.), The SINMAP approach to terrain stability mapping. Proceedings of the 8th Congress of International Association of Engineering Geology and the Environment, vol. 2. A. A. Balkema, Rotterdam, pp. 1157–1165.
Pack, R.T., Tarboton, D.G., Goodwin, C.N., 1998b. Terrain stability mapping with SINMAP. Technical description and user's guide for version 1.00. Report No. 4114-0. Terratech Consulting Ltd., Salmon Arm, B.C., Canada.
Pack, R.T., Tarboton, D.G., Goodwin, C.N., Prasad, A., 2005. SINMAP 2, a stability index approach to terrain stability hazard mapping. Technical Description and User's Manual for version 2.0. Utah State University, USA.
Peck, R.B., 1959. Report on Causes and Remedial Measures, Waiomao Slide, Honolulu. Unpublished Report to the City and County of Honolulu, 31 pp.
Peck, R.B., 1967. Stability of natural slopes. Journal of the Soil Mechanics and Foundation Division, ASCE, 93 (SM4), 403–418.
Peck, R.B., 1968. Supplementary Report on Remedial Measures, Waiomao Slide, Honolulu. Unpublished report to the City and County of Honolulu, 35 pp.
Peck, R.B., Wilson, S.D., 1968. The Hind luka landslide and similar movements, Honolulu, Hawaii. Unpublished report to the City and County of Honolulu, Hawaii, USA. 21 pp.
Peterson, D.M., Ellen, S.D., Knifong, D.L., 1993. Distribution of past debris flows and other rapid slope movements from natural hillslopes in the Honolulu District of Oahu, Hawaii. Open File Report. U.S. Geological Survey, pp. 93–514.
Scott, G.A.J., 1969. Relationships between vegetation and soil avalanching in the high rainfall areas of Oahu, Hawaii. M.A. Thesis, University of Hawaii, Honolulu, Hawaii, USA.
Scott, G.A.J., Street, J.M., 1976. The role of chemical weathering in the formation of Hawaiian amphitheatre-headed valleys. Zeitschrift für Geomorphologie 20, 171–189.
State of Hawaii, 1988. Post Flood Report, New Year's Eve Storm, December 31, 1987–January 1, 1988, Windward and Leeward East Oahu. Department of Land and Natural Resources, State of Hawaii. Circular C119. 55 pp.
Stearns, H.T., 1939. Geologic map and guide of the island of Oahu, Hawaii. Territory of Hawaii, Division of Hydrography Bulletin 2, 1–75.
Streans, H.T., Vaksvik, K.N., 1935. Geology and ground-water resources of the island of Oahu. Territory of Hawaii Division of Hydrography Bulletin 1, 1–479.
Torikai, J.D., Wilson, R.C., 1992. Hourly rainfall and reported debris flows for selected storm periods, 1935–91, in and near the Honolulu District, Hawaii. Open File Report. U.S. Geological Survey, pp. 92–486.
Tsukamoto, Y., Kusakabe, O., 1984. Vegetation influences on debris slide occurrences on steep slopes in Japan. In: O'Loughlin, C.L., Pearce, A.J. (Eds.), Symposium on Effects of Forest Land Use on Erosion and Slope Stability. University of Hawaii East West Center Environmental and Policy Institute, Honolulu, pp. 63–72.
USDA, 1972. Soil Survey of Kauai, Oahu, Maui, Molokai, and Lanai. USDA-ARS, Washington, DC, USA.
Visher, F.N., Mink, J.F., 1964. Ground-water resources in Southern Oahu, Hawaii. Water-Supply-Paper, vol. 1778. U.S. Geological Survey. 133 pp.
Varnes, J., 1978. Slope movement types and processes. In: Schuster, R.L., Krizek, R.J. (Eds.), Landslide: Analysis and Control. Special Report, vol. 176. Transportation Research Board, Washington, DC, USA, pp. 11–33.
Wan, Y., Kwong, K., 2002. Shear strength of soils containing amorphous clay-size materials in a slow-moving landslide. Engineering Geology 65, 293–303.
Wentworth, C.K., 1943. Soil avalanches on Oahu, Hawaii. Geological Society of American Bulletin 54, 53–64.
Wilson, R.C., Torikai, J.D., Ellen, S.D., 1992. Development of rainfall warning thresholds for debris flows in the Honolulu District, Oahu, Hawaii. Open File Report. U.S. Geological Survey, pp. 92–521.
Wu, W., Sidle, R.C., 1995. A distributed slope stability model for steep forested watersheds. Water Resources Research 31, 2097–2110.
Zaitchik, B.F., van Es, H.M., 2003. Applying a GIS slope-stability model to site-specific landslide prevention in Honduras. Journal of Soil and Water Conservation 58, 45–53.
Zaitchik, B.F., van Es, H.M., Sullivan, P.J., 2003. Modeling slope stability in Honduras: parameter sensitivity and scale of aggregation. Soil Science Society of America Journal 67, 268–278.